Lepton distribution in rare B decays

Dongsheng Liu and R. Delbourgo
Department of Physics, University of Tasmania, Hobart, Australia 7005
(Received 22 July 1996; revised manuscript received 27 January 1997)

We study lepton distributions in flavor-changing neutral current induced B meson decays into a pair of light leptons along with strange states. In addition to the invariant mass distribution, we examine the polarization, forward-backward, and polarization forward-backward asymmetries of the final state leptons. The standard model predictions for these distributions are at a level which is accessible to the forthcoming B factories. We also investigate the consequence of extensions of the standard model, including models with two Higgs doublets and supersymmetric extensions. Substantial deviations in individual distributions are found in certain regions of the parameter space of specific models. Therefore confronting these findings with future measurements may either highlight new physics or place constraints on extensions beyond the standard model. We derive results determined by the structure of the effective Hamiltonian which is common to the standard model and other models, independently of the values of couplings which can vary from model to model. [S0556-2821(97)05809-8]

PACS number(s): 13.20.He, 11.30.Ly, 11.40.Ex, 12.60.Rc

I. INTRODUCTION

Flavor-changing neutral-current- (FCNC-) induced dilepton B decays, like their radiative counterparts, proceed through loop diagrams within the standard model and thus are sensitive to new physics. The recent measurement of $B\to X_s\gamma$ by the CLEO group [1] results in constraints on the parameter space of extensions of the standard model [2]. Present searches for FCNC decays into final dileptons have set an upper limit within a factor of 3 of the branching ratio predicted by the standard model [3]. We expect that forthcoming experiments in the current B facilities and at future B factories will offer much more information about these leptonic channels. Because of the several sources which can lead to these decays, including even the long-distance contribution from J/ψ and ψ' resonances, the proper method of isolating different effects in the dileptonic channel is to measure a number of kinematic distributions of the final state particles. So far, apart from extensive studies about the invariant mass spectrum of dileptons, there is published work on the leptonic polarization [4,5], forward-backward asymmetry [6–9], the lepton-antilepton energy asymmetry [10], and the polarization of K^* in the exclusive channel [11]. In this paper, we present our analysis for the leptonic distributions and asymmetries in the decay $B\to X_s l^+ l^-$ ($l=e$ and μ) within and beyond the standard model.

As most of the phase space of the transition $B\to X_s$ has momentum transfer much greater than the mass of light leptons, we will evaluate our amplitudes in the limit of $m_l\to 0$ and neglect the mixting between the left- and right-handed leptons when it is appropriate to consider the decay distributions in terms of the lepton handness. At the same time we want to account for the angular distribution of lepton production. We shall derive the decay distribution for left-handed leptons over all angles and their right-handed counterpart. However, the practical observables are the invariant mass spectrum of dileptons which is obtained by summing these handed components in the forward and backward directions separately; from these four distributions, we also obtain polarization, forward-backward, and polarization forward-backward double asymmetries corresponding to three separate differences. To our knowledge, the polarization forward-backward asymmetry of lepton production in the $B\to X_s l^+ l^-$ is considered for the first time in the context of the standard model as well as its extensions. The effect of the two-Higgs-doublet model I on the dilepton decay width has been studied previously [12,13]. We now reexamine the subject in the light of a tightly constrained parameter space induced by the recent measurements of $\mathcal{B}(B\to X_s\gamma)$ and m_t. Interestingly, the constrained model I is still able to increase $\Gamma_{l^+l^-}$ substantially; the prediction changes slightly with the mass of the charged Higgs boson. (Model II is embraced by supersymmetric models.) Although the polarization of light leptons has been studied in the standard model, it has not yet been examined in the context of extended models, especially in supersymmetric ones. We thus consider the polarization in a number of extended models of electroweak interactions. Ali, Giudice, and Mannel have attempted to study the impact of a supersymmetric model on the $B\to X_s l^+ l^-$, but they mainly concentrated on the parameter space [8]. Here we present the direct consequence of the supersymmetric model on individual lepton distributions. Moreover, we are able to derive results which are the consequences of the structure of an effective Hamiltonian for the transition $B\to X_s$ and thus apply not only to the standard model, but also to a large number of its extensions. For instance, we find that the lepton polarization approaches twice as large as the forward-backward asymmetry at the upper boundary of the phase space and the polarization forward-backward asymmetry (normalized to the width) goes to $-3/4$ at the lower boundary. Also, we propose a method for determining experimentally the short-distance coefficients (both their magnitudes and signs) governing the $B\to X_s$ transition, using a dilepton invariant mass spectrum along with asymmetries yet to be measured. By following such a procedure, we are able to probe new physics in a model-independent way. We do not consider the $\tau^+\tau^-$ channel here for two reasons: first, the phase space is limited and appreciably reduces the

branching fraction; second, the left- and right-handed chiral projections do not quite correspond to helicities for massive leptons, and so the kinematics is rather more complicated.

In the following section we shall set out the formalism. After a brief review of an effective Hamiltonian inducing the transition $b\to s$, we summarize the expressions of the differential distributions of decay width, polarization, forward-backward, and polarization forward-backward asymmetries. In Sec. III we report model calculations of these distributions, corresponding to (i) the standard model, (ii) a model with two Higgs doublets of type I, and (iii) the supersymmetric extension of the standard model in the context of minimal supergravity with radiative breaking of SU(2)×U(1). We highlight model-independent results in Sec. IV as well as describing a proposal to determine the coefficients for the effective Hamiltonian experimentally. The last section is devoted to conclusions. The coefficients arising from nonstandard models are presented in the Appendix.

II. LEPTON DISTRIBUTIONS AND ASYMMETRIES

Let us begin with an effective Hamiltonian relevant to flavor-changing neutral current processes $b(P)\to s(p)l^+(p_1)l^-(p_2)$ [14]:

$$H_{\rm eff}=\frac{G_F}{\sqrt{2}}\left(\frac{\alpha}{4\pi s_W^2}\right)[\overline{s\Gamma}^A_\mu b\overline{l\gamma}^\mu(1-\gamma_5)l + \overline{s\Gamma}^B_\mu b\overline{l\gamma}^\mu(1+\gamma_5)l], \quad (1)$$

with the effective vertex $\Gamma^A_\mu=A\gamma_\mu(1-\gamma_5) - im_b s_W^2 F_2\sigma_{\mu\nu}q^\nu(1+\gamma_5)/q^2$ and Γ^B_μ is obtained by substituting B for A. Here s_W denotes $\sin\theta_W$, θ_W being the weak mixing angle, m_b is the mass of the bottom quark, and $q=(p_1+p_2)$, is the total momentum of the outgoing lepton pair. The fine structure constant of electromagnetic interaction α takes a value of 1/133 at the mass scale of the bottom quark. In the standard model, the F_2 term arises from the *photon penguin* diagram in which the W boson and top quark circulate. It is necessarily the same for left- and right-handed leptons in order to produce a purely vectorial interaction at the photon end, while the $(1+\gamma_5)$ factor at the quark end is dictated by the handedness of the quarks. The CLEO measurement of $B\to X_s\gamma$ results in a constraint on the magnitude of F_2, which is consistent with the value of the standard model and leaves limited room for new physics. Because they are absent in the radiative decays, the coefficients A and B can only be tested in dilepton processes. However, as A (and B) consists of several parts associated with different contributions, to obtain bounds on the parameters for extensions of the standard model from experiments needs some degree of sophistication. For the sake of a precise description, it is appropriate to decompose these two coefficients into

$$A=A_1+A_2+\sum_V A_V, \quad B=B_1+B_2+\sum_V B_V, \quad (2)$$

where the short-distance components A_1 and B_1 represent the contribution of heavy particles such as top quarks and W,Z bosons in the standard model. They are very sensitive to new physics and take different values in different models. We divide them further into two parts, writing them in the form $A_1=A_1^{\rm SM}+A_1'$ (the same applies to B_1). Here $A_1^{\rm SM}$ ($B_1^{\rm SM}$) accounts for the contribution of the standard model [15], which we shall always include in what follows. The effects of new physics (whatsoever the source) are represented by A_1' (B_1'). The term A_2 ($=B_2$) arises from the additive QCD renormalization and the loops of light quarks active at an energy scale of about 1 GeV [12]. It is independent of schemes as explicitly demonstrated at next-to-leading order by the authers of Refs. [16, 17]. This part is related to the low energy scale and, we believe, remains unchanged in extensions of the standard model when no new operators are introduced. (By contrast, in certain extensions such as left-right symmetric models low energy operators are also changed.) Finally, the contribution of vector resonances such as J/ψ and ψ' via current-current four-quark operators are taken into account by A_V ($=B_V$), which may be given by vector-meson dominance [18]. We point out that the difference between left- and right-handed leptons lies in the short-distance coefficients A_1 and B_1. In other words, the combination $A-B$ remains equal to its high energy scale value, A_1-B_1. In this work, we restrict ourselves into the structure of Eq. (1), which incorporates, in addition to the standard model, a number of new models such as the two-Higgs-doublet model and a minimal supersymmetric model. Allowing for nonzero inputs of A_1' and B_1' in extensions of the standard model, we are able to study the consequences of new physics in the decay $B\to X_s l^+l^-$, in terms of different decay distributions or, put another way, we derive bounds on A_1' and B_1' and, consequently, constraints on new models by using these distributions when they become available experimentally.

Let us now consider the decay distributions. With the Γ^A sector of Eq. (1), a double-differential distribution in the Dalitz plot for left-handed leptons is calculated to be

$$\frac{d\Gamma_L}{ds\,dx}=\frac{G_F^2 m_b^5}{16\pi^3}\left(\frac{\alpha}{4\pi s_W^2}\right)^2\left\{|A|^2\left[\frac{1}{4}(1-s^2)-x^2-sx\right] + \frac{1}{s}|C|^2\left[\frac{1}{4}(1-s^2)+x^2+x\right] + 2\,{\rm Re}(A^*C)\left[\frac{1}{2}(1-s)-x\right]\right\}, \quad (3)$$

where $C\equiv s_W^2F_2$. In this form we have ignored the mass of the strange quark and measured s in units of m_b^2 so that the squared invariant mass of the dilepton ranges over $(2m_l/m_b)^2\leq s\leq 1$. Also, x stands for $k\cdot p/m_b^2$ with $k=p_1-p_2$, ranging from $-(1-s)/2$ to $(1-s)/2$. If the (l^+l^-) frame is specified, the ratio $2x/(1-s)$ turns out to be $\cos\theta_l$ where π-θ_l is the polar angle of the l^+ with respect to the direction of motion of the decaying particle. Such an effect disappears in the s distribution obtained by integrating over x and can only be detected by measurements of angular distributions such as a forward-backward asymmetry. To obtain a corresponding result for right-handed leptons substi-

tute B for A in Eq. (3) and flip the sign of terms linear in x. Now we are in a position to write out individual distributions.

First, the differential decay width in the dilepton invariant mass squared reads

$$\frac{1}{\Gamma_{\rm sl}}\frac{d\Gamma}{ds}=\frac{1}{8\pi^2|V_{bc}|^2\tilde{f}_{bc}}\left(\frac{\alpha}{s_W^2}\right)^2(1-s)^2\Bigg[(1+2s)(|A|^2+|B|^2)+2\left(1+\frac{2}{s}\right)|C|^2+6\,\mathrm{Re}[(A+B)^*C]\Bigg], \tag{4}$$

with $\Gamma=\Gamma_R+\Gamma_L$. This distribution is normalized to the width of the semileptonic B decay $\Gamma_{\rm sl}$ dominated by the process $b\to c l\bar{\nu}_l$. $\Gamma_{\rm sl}$ itself contains m_b^5 and thereby eliminates the uncertainty that is highly sensitive to the bottom quark mass; nevertheless, there is moderate dependence of $\tilde{f}_{bc}$ on m_b, a product of the phase space factor and the one-loop QCD correction to the semileptonic B decay, which will be taken equal to 0.39 numerically in this work. In addition, we obtain the differential distribution for the lepton polarization:

$$\frac{1}{\Gamma_{\rm sl}}\frac{d\Gamma^{\rm pol}}{ds}=\frac{1}{8\pi^2|V_{bc}|^2\tilde{f}_{bc}}\left(\frac{\alpha}{s_W^2}\right)^2(1-s)^2[(1+2s)(|B|^2-|A|^2)+6\,\mathrm{Re}[(B-A)^*C]], \tag{5}$$

with $\Gamma^{\rm pol}=\Gamma_R-\Gamma_L$. Clearly, it is a parity-violating effect revealed by the overall factor A-B, which depends solely on the short-distance coefficients. So we expect that the lepton polarization will play a particular role in probing new physics of the high energy scale. Because there is no singularity at $s=0$ in Eq. (5) the polarization difference between electron and muon channels is negligible. In the μ channel this polarization should be readily found via the energy distributions of the decay products in the subsequent μ decays, which depend on the μ polarization. However, for the e channel this may be a little more difficult to test experimentally as the efficiency is usually rather low.

The differential forward-backward asymmetry of the l^+ production that we are to consider is defined by

$$d\Gamma_{\rm FB}(s)=\int_0^1 d\Gamma(\cos\,\theta_l)-\int_{-1}^0 d\Gamma(\cos\,\theta_l),$$

where the z axis is along the direction of the bottom quark in the center-of-mass frame of the lepton pair. It involves the chirality of lepton currents and takes the form

$$\frac{1}{\Gamma_{\rm sl}}\frac{d\Gamma_{\rm FB}}{ds}=\frac{1}{8\pi^2|V_{bc}|^2\tilde{f}_{bc}}\left(\frac{\alpha}{s_W^2}\right)^2(1-s)^2\Bigg[\frac{3}{2}\,s(|B|^2-|A|^2)+3\,\mathrm{Re}[(B-A)^*C]\Bigg]. \tag{6}$$

It is also proportional to the combination A-B and should become an effective test of new physics. In parallel, we define the polarization forward-backward asymmetry as

$$d\Gamma_{\rm FB}^{\rm pol}(s)=\int_0^1 d\Gamma^{\rm pol}(\cos\,\theta_l)-\int_{-1}^0 d\Gamma^{\rm pol}(\cos\,\theta_l),$$

which is derived to have the form

$$\frac{1}{\Gamma_{\rm sl}}\frac{d\Gamma_{\rm FB}^{\rm pol}}{ds}=\frac{1}{8\pi^2|V_{bc}|^2\tilde{f}_{bc}}\left(\frac{\alpha}{s_W^2}\right)^2(1-s)^2\Bigg[\frac{3}{2}\,s(|A|^2+|B|^2)-\frac{3}{s}\,|C|^2+3\,\mathrm{Re}[(A+B)^*C]\Bigg]. \tag{7}$$

Note that the dependence on the coefficient functions in the equation is analogous to that in Eq. (4). As far as the μ channel is concerned, the polarization forward-backward asymmetry of the μ^+ production may be indirectly measured via the correlation between the decay distributions of the $\mu^+\mu^-$ pair as the decay distribution of a single lepton only depends on its polarization.

III. MODEL PREDICTIONS

A. Lepton distributions in the standard model

The standard model calculation for the coefficients in the effective Hamiltonian of Eq. (1) has been carried out in many works. It is well known now that the main contribution to $B\to X_s l^+ l^-$ arises from the photon penguin, Z boson penguin, and W boson box diagrams. Given the large top quark mass, namely, $m_t=175.2$ GeV, obtained by averaging the data of Collider Detector at Fermilab (CDF) and D0 groups [19], the Z boson penguin along with W boson box diagrams take over the the photon penguin one, except near $s\simeq 0$. Measurements of the dilepton process offer an opportunity to test aspects of the standard model which are hardly detectable in radiative decays. For $A_1^{\rm SM}$ and $B_1^{\rm SM}$, we will use their explicit form given in Refs. [14,15],

$$A_1^{\rm SM}=V_{ts}^*V_{tb}A_t,\quad B_1^{\rm SM}=V_{ts}^*V_{tb}B_t, \tag{8}$$

where V_{ts} and V_{tb} are Cabibbo-Kobayashi-Maskawa (CKM) matrix elements. At the energy scale equal to the W boson mass, A_t and B_t take the forms (with $x=m_t^2/M_W^2$)

$$A_t(x,1)=B_t(x,1)+\frac{1}{4}\left[x+\frac{3x}{1-x}+\frac{3x^2}{(1-x)^2}\,\ln x\right],$$

$$B_t(x,1)=-\Bigg[\frac{1}{2}\,x+\frac{3}{4}\,\frac{x}{1-x}+\frac{3}{4}\,\frac{2x^2-x}{(1-x)^2}\,\ln x-\frac{4}{9}\,(\ln x+1)+\frac{1}{36}\,\frac{82x^3-151x^2+63x}{(1-x)^3}+\frac{1}{36}\,\frac{10x^4+59x^3-138x^2+63x}{(1-x)^4}\,\ln x\Bigg]s_W^2. \tag{9}$$

The current-current and gluon penguin four-quark operators also give rise to A and B through the mixing due to the QCD renormalization. From unitarity of the CKM matrix, we have

$$A_2 = V_{ts}^* V_{tb}(A_{\rm QCD} - A_f),$$

when $V_{us}^* V_{ub}$ is negligible. The evaluation of $A_{\rm QCD}$ has been performed at next-to-leading order by the authors of Refs. [16,17]. Here we adopt their results in the naive dimension reduction (NDR) scheme:

$$A_{\rm QCD}(\eta) = -s_W^2 \sum_{i=1}^{6} \left[\left(\frac{\pi}{\alpha_s(M_W)}\, p_i + s_i \right)(1-\eta^{-a_i-1}) + r_i(1-\eta^{-a_i}) \right],$$

where the scale-dependent parameter $\eta = \alpha_s(\mu)/\alpha_s(M_W)$, with $\alpha_s(M_W)$ taking a value of 0.120. The effect arising from the one-loop matrix elements of the four-quark operators is given by

$$A_f = s_W^2 \left[(a_2 + a_4 + a_6)\,\phi(m_c^2/m_b^2, q^2/m_b^2) - \frac{a_3 + a_4 + a_6}{2} \times \phi(1, q^2/m_b^2) - \frac{a_3}{2}\,\phi(0, q^2/m_b^2) - \frac{2}{3}\,(a_4 + a_6) \right],$$

where $a_2 = c_1 + c_2/3$, $a_3 = c_3/3 + c_4$, $a_4 = c_3 + c_4/3$, $a_6 = c_5 + c_6/3$, and the function ϕ reads

$$\phi(r_q, s) = \begin{cases} \dfrac{4}{3}\ln r_q - \dfrac{8}{9} - \dfrac{4}{3}\dfrac{4r_q}{s} + \dfrac{2}{3}\sqrt{1-\dfrac{4r_q}{s}}\left(2+\dfrac{4r_q}{s}\right)\left(\ln\dfrac{1+\sqrt{1-4r_q/s}}{1-\sqrt{1-4r_q/s}} - i\pi\right) & \left(\dfrac{4r_q}{s} < 1\right) \\ \dfrac{4}{3}\ln r_q - \dfrac{8}{9} - \dfrac{4}{3}\dfrac{4r_q}{s} + \dfrac{4}{3}\sqrt{\dfrac{4r_q}{s}-1}\left(2+\dfrac{4r_q}{s}\right)\arctan\dfrac{1}{\sqrt{4r_q/s-1}} & \left(\dfrac{4r_q}{s} > 1\right) \end{cases}.$$

When $\eta = 1$ corresponding to $\mu = M_W$, one has $a_2 = 1/3$ and $a_3 = a_4 = a_6 = 0$. The QCD renormalization decreases a_2 and gives rise to the other coefficients. Nevertheless, the charm quark essentially dominates the effect of these active quarks at the scale near the bottom quark mass, as indicated by the numerical values of these coefficients for $\eta = 1.75$. As for the long-distance effects arising from vector resonances, we shall follow the notation of Ref. [9]:

$$A_V = \frac{16\pi^2}{3}\left(\frac{f_V}{M_V}\right)^2 V_{cs}^* V_{cb}\,\frac{a_2 s_W^2}{q^2 - M_V^2 + iM_V\Gamma_V}.$$

Last but not least, the magnetic-moment operator has nonzero anomalous dimension and mixes with other operators; the coefficient for it is given by $F_2 = F_2' + V_{ts}^* V_{tb} F_2^t$, where [16]

$$F_2^t(x,\eta) = \eta^{-16/23}\left[\frac{1}{12}\frac{8x^3+5x^2-7x}{(1-x)^3} + \frac{1}{2}\frac{3x^3-2x^2}{(1-x)^4}\ln x + (\eta^{2/23}-1)\left(\frac{2}{3}\frac{x^3-5x^2-2x}{(1-x)^3} - \frac{4x^2}{(1-x)^4}\ln x \right) \right] + 2\sum_{i=1}^{8} h_i \eta^{-a_i}. \quad (10)$$

Here F_2' (switched off in this section) represents the magnetic-moment form factor arising from extensions of the standard model. It mixes with the chromomagnetic Pauli interaction as the energy scale goes down, but this mixing is actually rather weak; for instance, $\eta^{2/23} - 1$ is merely 5% for $\eta = 1.75$.

The standard model predictions for the leptonic distributions discussed in the previous section are summarized in Figs. 1 and 2. In Fig. 1(a), we plot the differential decay width of the the $B \to X_s l^+ l^-$. Obviously, the soft photon penguin governs the region $s \simeq 0$. Thus measurements of the distribution in this region provide a cross-check of the magnetic-moment operator. The two pronounced peaks in the middle region correspond to the contributions of the J/ψ and ψ' via $V \to l^+ l^-$. They are insensitive to short-distance physics, but dominate the *integrated* width of the $B \to X_s l^+ l^-$. To probe the effects of $A_1^{\rm SM}$ and $B_1^{\rm SM}$ on the spectrum, we have to examine the regions outside these peaks. As we can see in Fig. 1(a), the photon and vector poles are relatively localized and we are left with three windows to observe the effects of the short-distance components of $A_{1,2}$ and $B_{1,2}$. The first window is the region above the ψ' resonance, say, $s \geq 0.65$, where the left-handed magnetic-moment operator enters mainly through interference which slightly lower the differential rate; the ψ' resonance has very limited impact. We believe that this region may be one of the ideal places where the decay behavior is determined by the short-distance physics and where we can compare the model prediction with experimental measurements, in spite of the fact that the phase space tends to be small there. In the second window, namely, the region between the two resonances, the situation is more involved. Although the contributions of $A_1 + A_2$ and $B_1 + B_2$ are important, the interference between them and A_V (B_V) along with F_2 has much more influence on the spectrum. We may make the third window by a cut below the J/ψ peak and by excluding the very small s region. The measurement of the lepton spectrum in this region will not only provide information about

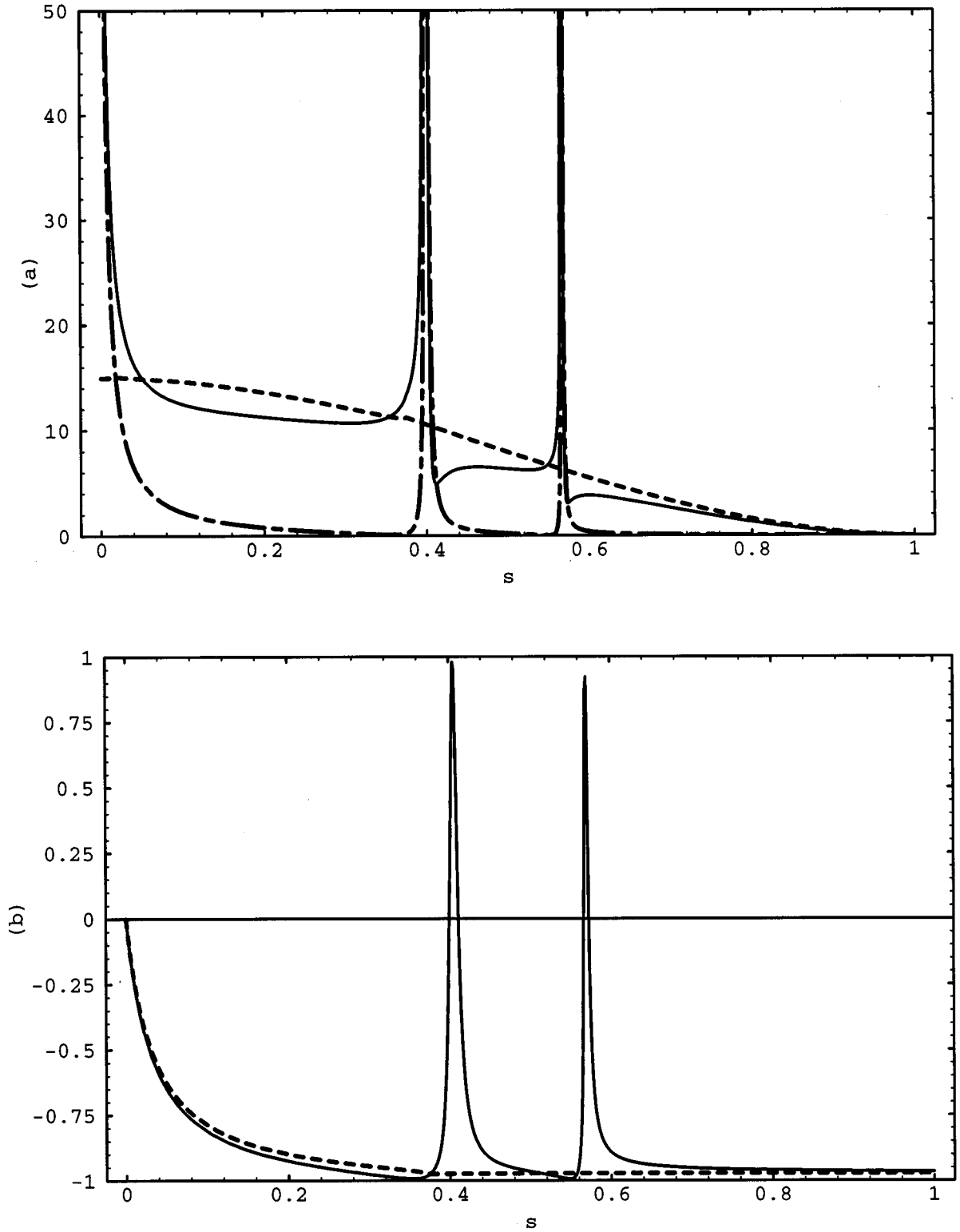

FIG. 1. (a) The standard model prediction for the differential decay width of the $B \to X_s l^+ l^-$ in the dilepton invariant mass squared in units of m_b^2 (solid line); the dashed line corresponds to the contribution solely from the coefficients $A_1 + A_2$ and $B_1 + B_2$, while the dot-dashed line stands for the contribution of the vector resonances along with the photon penguin diagram, namely, the F_2 term of Eq. (1) (all plots are rescaled by the semileptonic decay width of the B meson, multiplied by the factor of 10^5), and (b) the differential distribution of lepton polarization normalized to differential decay width, $(d\Gamma^{\rm pol}/ds)/(d\Gamma/ds)$, in the standard model with (solid line) and without (dashed line) vector resonances.

the short-distance components of A and B, but also help us to determine the relative sign between the coefficient F_2 and $A_1^{\rm SM}$ or $B_1^{\rm SM}$ as the interference between them becomes substantial.

The differential distribution of lepton polarization, normalized to differential decay width, is plotted in Fig. 1(b). As we know, it scales as A-B and thus reveals the short-distance physics even in the vector resonant region. Note that the polarization is sizable and negative in most of the phase space, which indicates left-handed lepton dominance, except for the two resonance and $s\simeq 0$ regions; note also that at the actual resonance peaks the polarization is negligible as it is near the photon mass shell. This means that the integrated polarization over the three ranges stated above is comparable to the corresponding integrated width.

The forward-backward asymmetry in Fig. 2(a) is likewise governed by A-B, vanishing at the exact resonance peaks; at the extreme limit $s=1$, it is predicted to be exactly $-1/2$ for the left-handed leptons as can be checked by taking the ratio of Eqs. (6) and (4). There is a small region near $s=0$ where the forward-backward asymmetry is positive, however, revealing the contribution of the photon penguin. So far as Fig. 2(b) is concerned the resonance peaks almost cancel out of the ratio of Eq. (7) to Eq. (4), which is a nice feature as it washes out the spikes in the resonant region to a large degree. Once again, there is a prediction that as $s\to 1$ this particular asymmetry tends to 1/2 as the effect of the photon penguin is bounded in the samll s region, where we have $-3/4$ regardless of the actual values of the coefficients.

Finally, we observe that with respect to integrals over s of asymmetries expressed in Eqs. (5) and (6), the polarization asymmetry is much more significant than the forward-backward asymmetry; the latter suffers from cancellation in the small s region and is about half of the former in the $s\simeq 1$ region.

B. Effects of charged Higgs bosons

In models with two Higgs doublets, there is a pair of physically charged Higgs particles, which can add to the W boson contribution in the loops of the standard model, giving rise to extra diagrams inducing the FCNC B decay [20–23]. In this situation, two additional parameters enter the analysis; one is the mass of the charged Higgs boson m_{H^-}, and the other is the ratio of the vacuum expectation values $v_{21}=v_2/v_1$ associated with the two neutral scalar Higgs bosons ϕ_1^0 and ϕ_2^0. Here we investigate the consequences of two versions (I and II) of two-Higgs-doublet models, where the FCNC is absent at the tree level. In model I it is ϕ_1^0 that is involved in Yukawa couplings and gives rise to the mass of all quarks, while ϕ_2^0 decouples from them. In model II, by contrast, ϕ_1^0 generates the mass of the up-type quarks and ϕ_2^0 is responsible for the mass of down-type quarks.

Let us consider model I first. In this case the interactions of the charged Higgs bosons with quarks are proportional to the ratio of the two vacuum expectation values and as a result the loop amplitude of the FCNC B decay grows quadratically with v_{21}. Depending upon v_{21} and m_{H^-}, the additional photon penguin diagram can either enhance or suppress the FCNC radiative B decay rate over the standard model. Consequently, the CLEO data of the $B\to X_s\gamma$ allows two separate regions in the parameter plane of model I [2,24]. One is a band with moderate $v_{21}\sim 2$ for $m_{H^-}=100$ GeV (referred to as the α region hereafter), which will shrink as the measurement is improved; the other (β region) is presently consistent with vanishing v_{21}. Note that there is no actual bound on the mass of charged Higgs bosons in both of them. Our scheme of choosing parameters in the α region is as follows. We define a path in the v_{21}-m_{H^-} plane for the α region such that it reproduces the mean value of the CLEO data, namely, $\mathcal{B}(B\to X_s\gamma)=2.32\times 10^{-4}$. Given the masses of charged Higgs bosons, v_{21} is fixed (or conversely). We regard the path as a representative of the α region and observe that both A_1' and B_1' add considerably and constructively to $A_1^{\rm SM}$ and $B_1^{\rm SM}$ for a large range of the m_{H^-} from 50 GeV to 1600 GeV. In fact, once v_{21} satisfies the constraint of fixed rate of the $B\to X_s\gamma$, the leading term of A_1' and B_1' (see the Appendix) for large charged Higgs boson mass $(\ln m_{\rm H^-}^2)/m_{\rm H^-}^2$ cancels out and these two coefficients are approximately independent of $m_{\rm H^-}$ as it becomes heavy along the particular path in the $m_{\rm H^-}$–v_{21} plane. Moreover, the interference in Eq. (4) becomes constructive. As a result, the invariant mass distribution of model I [see Fig. 3(a)] is *substantially* enhanced over that of the standard model in the three windows stated previously. This large enhancement in decay width was addressed by Grinstein, Savage, and Wise [12]. Here we have demonstrated that it still survives after practical constraints from the $B\to X_s\gamma$ are placed on the parameter plane. The integrated widths without the vector resonant contributions over the whole phase space are calculated to be $\Gamma_{ee}=29.6\times 10^{-5}\Gamma_{\rm sl}$ and $\Gamma_{\mu\mu}=27.6\times 10^{-5}\Gamma_{\rm sl}$ for $m_{\rm H^-}=100$ GeV. Using the CLEO 95% C.L. bounds on $\mathrm{B}(B\to X_s\gamma)$, we end up with ranges of $(24-36)\times 10^{-5}\Gamma_{\rm sl}$ and $(23-33)\times 10^{-5}\Gamma_{\rm sl}$ for the electron and muon channels, respectively. They are over a half of the current experimental upper limits. We have evaluated these widths for a range of the charged Higgs boson mass from 50 GeV to 1600 GeV and found that they decrease slightly with increasing $m_{\rm H^-}$. We may, therefore, regard the above predictions for the decay width as typical of the whole α region.

The distributions of lepton asymmetries are plotted in Fig. 3 for the same parameters. We observe that the polarization [see Fig. 3(b)] is reduced by the extra effects, apart from small s where it is enhanced in magnitude (the resonant region is hardly affected, of course). The forward-backward asymmetry [Fig. 3(c)] for $s\simeq 0$ reverses its sign and there is no longer cancellation when we integrate. Since the short-distance component is enhanced overall, the contribution of vector resonances is accordingly less apparent in the polarization forward-backward asymmetry [Fig. 3(d)]. Interestingly, this particular asymmetry does not seem to change above the ψ' and is pinned down at the lower boundary of the phase space.

The situation for parameters falling in the β region on the v_{21}-m_{H^-} plane is distinctly different from the α region. The rate of the $B\to X_s\gamma$ with charged Higgs bosons is smaller than without them. Thus the CLEO lower limit at 95% C.L. $\mathcal{B}(B\to X_s\gamma)>1.0\times 10^{-4}$ sets up a boundary of this region. Only small v_{21} or heavy $m_{\rm H^-}$ is allowed. On the other hand, the $B\to X_s l^+ l^-$ rate, as we shall soon see, is enhanced by the

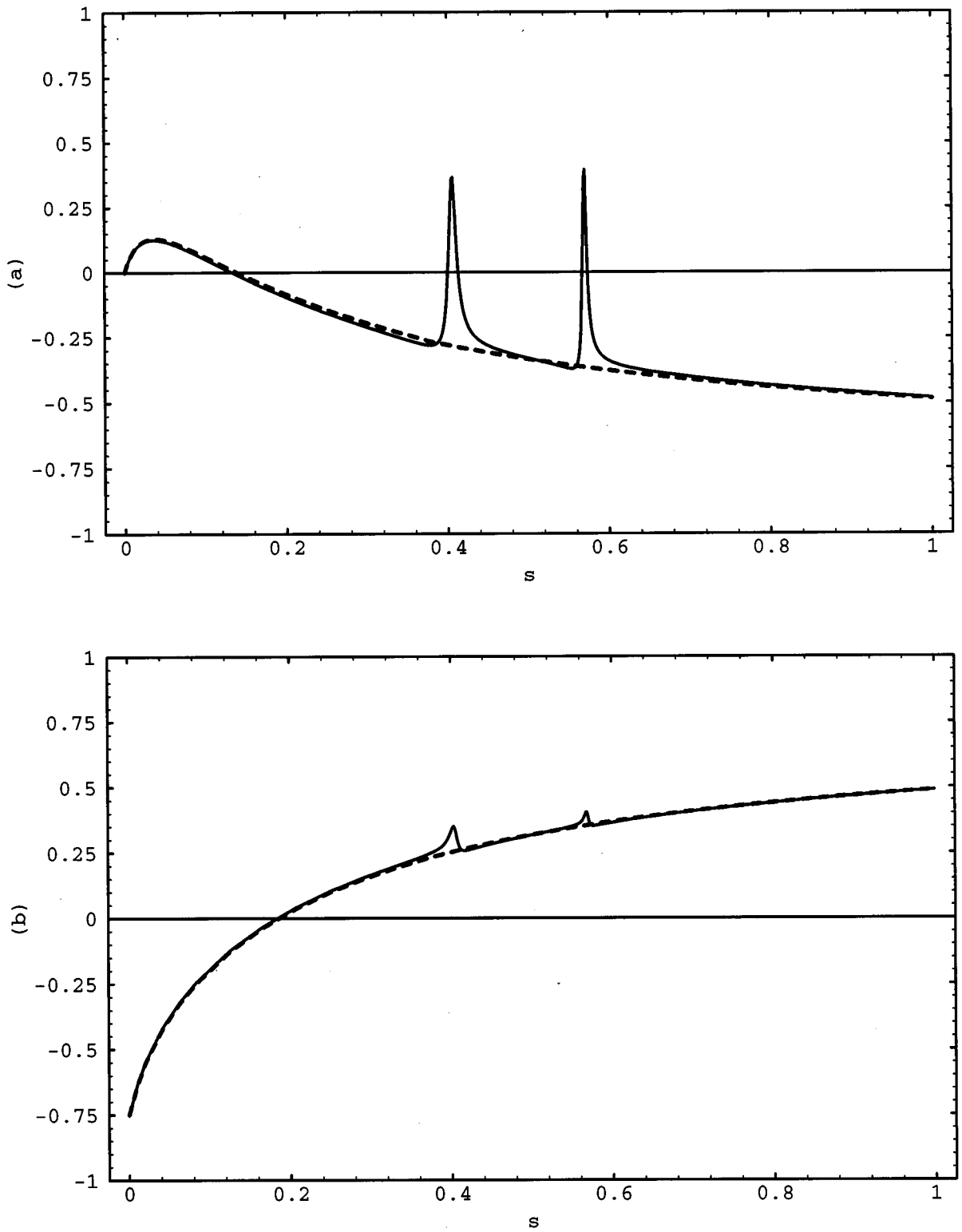

FIG. 2. (a) The differential distribution of the forward-backward asymmetry of the l^+ production in the l^+l^- frame, $(d\Gamma_{\rm FB}/ds)/(d\Gamma/ds)$, in the standard model with (solid line) and without (dashed line) vector resonances; (b) the same for the polarization forward-backward asymmetry of leptons, $(d\Gamma^{\rm pol}_{\rm FB}/ds)/(d\Gamma/ds)$.

charged Higgs boson contribution, but to a lesser extent. This is due to the fact that A_1' and B_1' still add constructively to $A_1^{\rm SM}$ and $B_1^{\rm SM}$ even though their magnitudes are strongly constrained by the measurements. Once again, we find that the A_1' and B_1' change slightly along the stated boundary and we expect the lepton distributions to be represented by a set of parameters on it, say, $m_{\rm H^-}=100$ GeV and the associated v_{21}. For them we plot the decay width and asymmetry distributions in Fig. 4.

The increase of about 50% in decay width of the μ channel may be compared with only 10% of the e channel. As far as FCNC dilepton B decays are concerned, it seems difficult

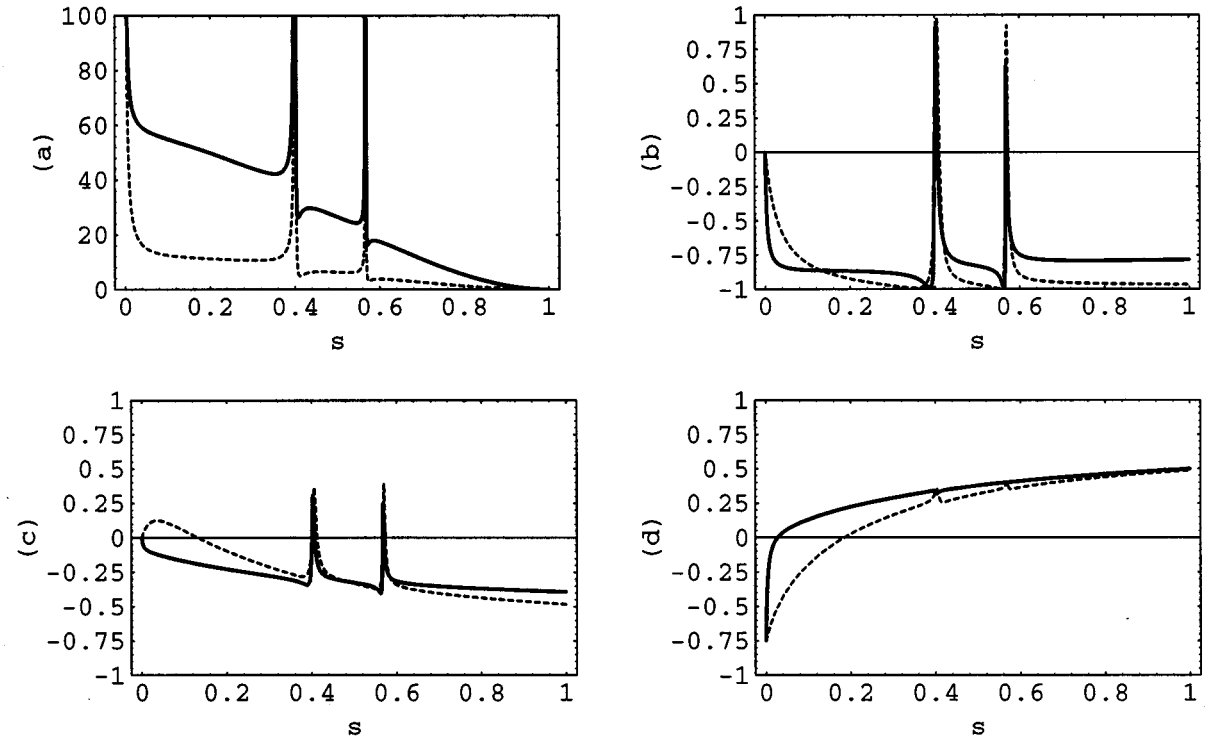

FIG. 3. The same as Figs. 1 and 2 for model I of the two-Higgs-doublet extension (solid line) of the standard model (dashed line), namely, (a) $d\Gamma/ds$ normalized to the semileptonic decay width of the B meson, (b) $(d\Gamma^{\rm pol}/ds)/(d\Gamma/ds)$, (c) $(d\Gamma_{\rm FB}/ds)/(d\Gamma/ds)$, and (d) $(d\Gamma^{\rm pol}_{\rm FB}/ds)/(d\Gamma/ds)$. The mass of the charged Higgs boson takes a value of 100 GeV and v_{21} (in the α region) is fixed by the CLEO date of $\mathcal{B}(B\to X_s\gamma)$.

to observe the consequence of further reducing v_{21} or heavy $m_{\rm H^-}$, unless there is a dramatic improvement in the calculation of the QCD renormalization and a high level of accuracy in measurements.

In model II, v_{21}^2 appears in the coupling of the charged Higgs bosons to left-handed quarks and $1/v_{21}^2$ in right-handed ones; they cancel out when they meet in the cross term of the photon penguin amplitude [21,22]. Hence we are left with a

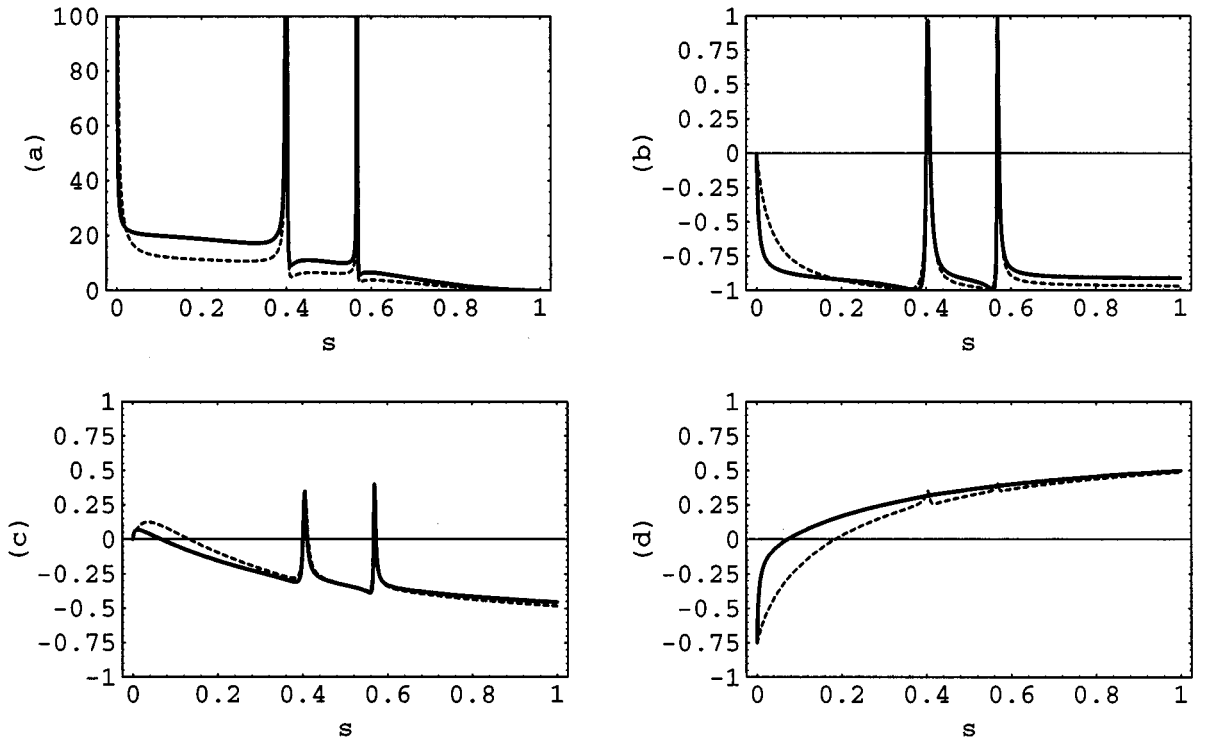

FIG. 4. The same as Fig. 3 for v_{21} in the β region.

v_{21}-independent part in the magnetic, monent form factor, which *enhances* the rate of $B\to X_s\gamma$ (as it does in the invariant mass spectrum for small s). This property leads to a lower bound on the charged Higgs boson mass in model II, regardless of the value of v_{21}, obtained from the CLEO data of the rate of the FCNC radiative B decay. The bound is far higher than that from the direct search at the CERN e^+e^- collider LEP [25]. But when the Higgs boson of model II is considered in the context of supersymmetric theory, as we shall do presently, its contribution to the decay $B\to X_s\gamma$ is sometimes destroyed by the chargino effect and the resulting experimental bound is modified dramatically. Moreover, the mass of charged Higgs bosons is no longer necessarily a free parameter; it may be evaluated in terms of other parameters. In the following subsection we continue our analysis by combining charged Higgs bosons arising from the supersymmetric extension of the standard model with other supersymmetric particles.

C. Minimal supergravity with radiative breaking of SU(2)×U(1)

In supersymmetric extensions of the standard model, such as minimal supersymmetry standard model (MSSM), loop diagrams of supersymmetric particles contribute to the FCNC B meson decays. The authors of Ref. [26] have presented a comprehensive analysis of the $B\to X_s$ transition in the context of the MSSM. They pointed out that in addition to W^--t and model II H^--t loops, there are chargino-up-squark (χ^--$\widetilde{U}$), gluino-down-squark, and neutralino-down-squark loops. Nevertheless, the latter two do not contribute to the process $B\to X_s l^+l^-$ as significantly as the others. This observation was recently confirmed by the authors of Ref. [10]. We shall not, therefore, consider them at the present stage. The short-distance (at the weak scale) coefficients arising from χ^--$\widetilde{U}$ diagrams computed in Refs. [10,26] are summarized in the Appendix. It should be remarked that the sign of the amplitude arising from the chargino box diagram in Ref. [26] differs from that in Ref. [10]. We notice that this amplitude turns out not to be substantial numerically and thus this sign discrepancy hardly impacts on our phenomenological analysis reported below. The partial width of the $B\to X_s l^+l^-$ has been investigated in Refs. [10,26] and we extend the study to various lepton distributions in this subsection.

Clearly, the analysis in the context of the supersymmetrized standard model involves many extra parameters in addition to the standard model parameters. Two of them come from the above stated charged Higgs boson contribution, being its mass and the ratio of the two neutral Higgs vacuum expectations, $\tan\beta\equiv 1/v_{21}$. The right-handed squarks of the first two generations are ignored since their effects are suppressed by a factor of $m_{u,c}/M_W$. We also notice that the $B\to X_s$ transition is insensitive to the mass difference of the (left-handed) up and charm squarks due to the small quark mixing V_{ub} compared with V_{tb}. As a result, provided no mixing occurs between or within these flavors, only one out of the four masses is important as far as first two generation up-type squarks are concerned. By contrast, we need to diagonalize the mass-squared matrix of left- and right-handed top squarks states, which has a rather large off-diagonal element due to the heavy top quark. Here one has two masses $m_{\tilde{t}_1}$ and $m_{\tilde{t}_2}$ along with a mixing angle $\theta_{\tilde{t}}$. The effects of charginos which are mass eigenstates of the W-ino and Higgsino, supersymmetric partners of the W and charged Higgs bosons, are parametrized by their masses and two mixing angles. As well, the supersymmetric counterpart of box diagrams involves the mass of the degenerate sneutrinos in the first two generations. Such a large number of parameters is undesirable when conducting a phenomenological study.

Like many others have done, we proceed to a further analysis in the context of the minimal supergravity theory with radiative breaking of SU(2)×U(1) [27]. In this theory three running gauge couplings meet each other at a unification scale M_X, which defines an universal coupling constant α_X. In practice, M_X along with α_X are determined by a fit of the three gauge couplings measured at m_Z via renormalization group equations of the minimal supersymmetric SU(3)×SU(2)×U(1) [28]. It is also assumed that the mass of every scalar particle runs and reaches a universal scalar mass m_0 at M_X, and so gaugino masses unify to $m_{1/2}$. Moreover, there is a common trilinear coupling A_0 for the soft scalar terms responsible for explicit supersymmetric breaking. Thus one has three parameters at M_X plus the $\tan\beta$ defined earlier at the weak scale which is the fourth parameter. Finally, the sign of the Higgs mixing parameter m_4 (which is sometimes denoted by μ in the literature) is free although its magnitude is fixed in terms of the measured m_Z along with the above four parameters. We take no account of the phases in A_0 and m_4 and assume R-parity conservation. The masses or mass matrices of supersymmetric particles at the weak scale are computed via one-loop renormalization group equations which determine the evolution of these masses below the unification scale. In this procedure we only take into account the Yukawa coupling of top quarks and restrict ourselves into $\tan\beta\leqslant 35$, above which the bottom quark Yukawa coupling is enhanced so much that it is comparable to the top quark one. On the other hand, to avoid a Landau pole of the top quark Yukawa coupling below the unification scale we have to set a lower limit of $\tan\beta\geqslant 1.98$ for a top quark mass of 175.2 GeV.

In the supersymmetry (SUSY) limit, namely, $m_{1/2}=m_4=0$ and $\tan\beta=1$, the magnetic operator cancels out, resulting in $\mathcal{B}(B\to X_s\gamma)=0$ [29]. This is in conflict with CLEO measurements of the rate of $B\to X_s\gamma$. Further, $\tan\beta=1$ leads to a Landau pole for the Yukawa coupling of the top quark. However, a partial cancellation between various contributions to the radiative decays of B mesons still occurs away from the SUSY limit due to the fact that in certain regions of the parameter space, especially for large values of $\tan\beta$ and $m_4>0$, the chargino loop amplitude has an opposite sign to that of the W and charged Higgs loops. Consequently, as the rate of the decay $B\to X_s\gamma$ is irrelevant to the sign of F_2, we cannot distinguish between two possible cases; one is the small deviation of F_2 from its standard model prediction within the current uncertainties of both experimental measurements and theoretical calculations. The other is a large deviation producing an F_2 of a similar magnitude, but opposite sign to the standard model. The measurement of $B\to X_s l^+l^-$ will enable us to disentangle the

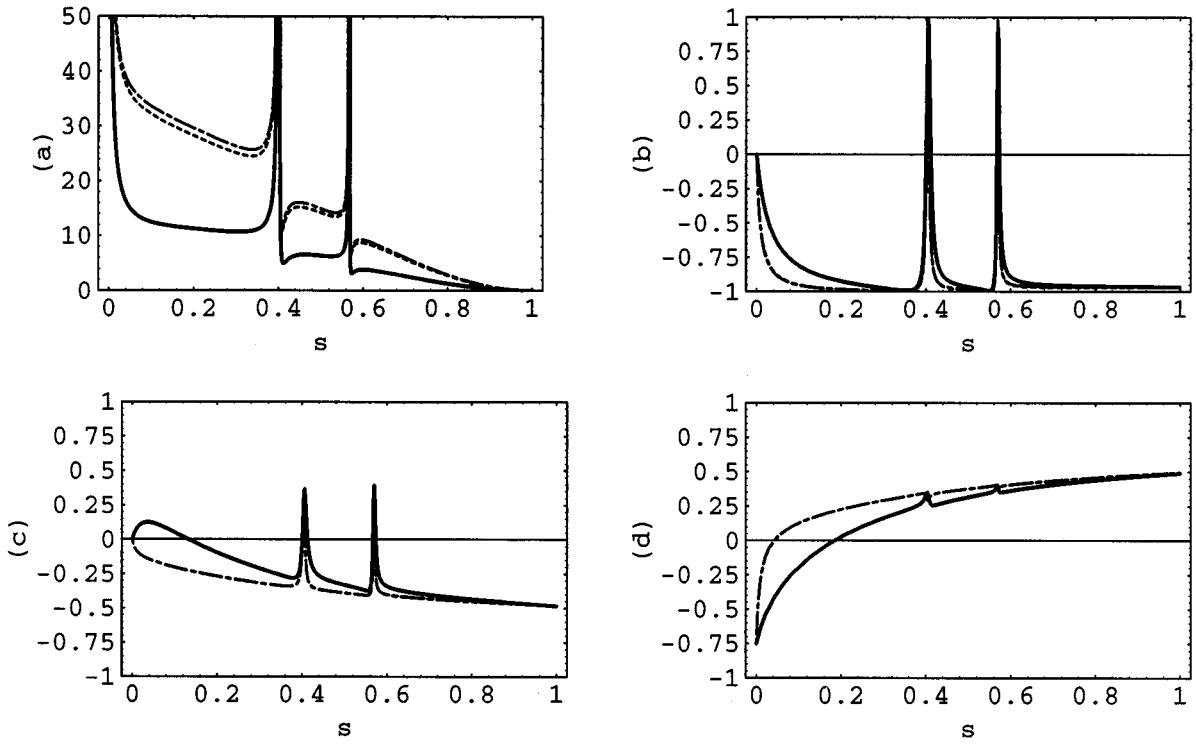

FIG. 5. The same as Fig. 3 for supersymmetric extensions of the standard model (solid line). The parameters are taken as (i) $m_{1/2}=100$ GeV, $m_0=300$ GeV, $A_0=2.50$, and $\tan\beta=18$ (dashed line); (ii) $m_{1/2}=120$ GeV, $m_0=300$ GeV, $A_0=2.65$, and $\tan\beta=28$ (dot-dashed line).

ambiguity as its width tends to be greater in the latter than in the former [8]. Therefore, large $\tan\beta$ is of particular interest, which enhances the effect of chargino loops in F_2' [30] and suppresses charged Higgs contributions to A_1' and B_1'. For $m_4>0$, we evaluate the lepton distributions for two representative sets of parameters; the first is chosen such that low-lying supersymmetric particles such as the light top squark and chargino are heavier than bounds set up by direct searches at LEP-1.5, but within the reach of LEP-2, namely, that $m_{\tilde{t}_1}=80.9$, $M_{\chi_1}=75.7$ (the light neutral scalar Higgs boson now has a mass about m_Z); the second results in the masses of all supersymmetric particles greater than 90 GeV, for example, $m_{\tilde{t}_1}=99.7$ and $M_{\chi_1}=92.9$.

Some remarks are in order: (1) These sets of parameters both repreduce the decay rates of the $B\to X_s\gamma$, agreeing with the CLEO data, but the resulting F_2 is now positive. (2) $A+B$ (mainly arising from chargino loops) changes less than 10%, while $A-B$ adds by about 50% constructively; the reason for this is that the dominant chargino loop is that of Z penguin type, for which the ratio of vector to axial vector lepton currents is $1-4s_W^2$. (3) In fact, if a squark mass is much greater than a chargino mass (or conversely) all amplitudes of chargino loops are finite, except for that of the Z penguin diagram which diverges logarithmically with the squark mass (the standard model Z penguin increases quadratically with the top quark mass).

Our numerical results are shown in Fig. 5. Obviously, we observe a large enhancement in the decay width distribution over the standard model prediction. The integrated widths without the vector resonant contributions over the whole phase space are calculated to be $\Gamma_{ee}=19.6(19.0)\times10^{-5}\Gamma_{\rm sl}$ and $\Gamma_{\mu\mu}=16.6(15.9)\times10^{-5}\Gamma_{\rm sl}$ for the first (second) set of parameters. The increase in decay width is roughly a factor of 2 and far beyond the uncertainty due to the calculation of QCD renormalization [16,17]. We increased m_0 to 500 GeV and 800 GeV, respectively, and correspondingly adjusted the value of A_0 to keep $m_{\tilde{t}_1}$ to be around 100 GeV, but we failed to find larger decay widths. Unlike the width, the deviations of asymmetries from the standard model prediction mainly occur in the small s region, say, below the J/ψ peak. With respect to polarization it seems that there is rarely a difference between the standard model and its supersymmetric extension when $s>0.2$. In the region above the ψ' resonance where the impact of the magnetic operator fades out, nearly complete lepton polarization (near -1) indicates that the left-handed lepton dominance is retained to a great extent after the effects of supersymmetric particles are taken into account, at least for the parameters used in this work. Forward-backward asymmetries flip their sign for $s\simeq0$, and as a result, an integrated asymmetry will be greatly enhanced. A sign change also occurs in polarization forward-backward asymmetries in the small s region. We may conclude that for the parameters used in this analysis all *integrated* asymmetries, like decay width, are enhanced in the supersymmetrized standard model.

We can also reverse the sign of m_4 for these two sets of parameters and find that the mass of top squarks is driven down to 28.1 GeV, well below the lower limit of LEP's direct searches and $\mathcal{B}(B\to X_s\gamma)$ almost reaches the CLEO upper limit at 95% C.L. in the first case, while in the second case $m_{\tilde{t}_1}$ drops to 76.6 GeV, but $\mathcal{B}(B\to X_s\gamma)$ violates the upper limit. In other words, a negative m_4 corresponding to these values of parameters is not viable.

IV. MODEL-INDEPENDENT ANALYSIS

In this section we first highlight results of lepton distributions which are not dependent on the specific values of the coefficients A, B, and F_2. Thus these results are regarded as consequences of the structure of the effective Hamiltinian of FCNC B decays in the context of standard model, as well as its supersymmetric extensions. We believe that violation of them, if observed in future experiments, can be regarded as evidence of new physics. We shall now show how to determine the three coefficients both in magnitude and in sign using the measurements of the width and asymmetries of the decay $B\to X_s l^+ l^-$ along with the width of the $B\to X_s\gamma$.

We begin by considering the polarization and forward-backward asymmetry, both of which measure the magnitude of the axial vector component of the lepton current $(A-B)$ interfering with the polar vector component. It is illuminating to write out the ratio

$$\frac{d\Gamma^{\rm pol}/ds}{d\Gamma_{\rm FB}/ds}=2\,\frac{(1+2s)(|B|^2-|A|^2)+6\,{\rm Re}[(B-A)^*C]}{3s(|B|^2-|A|^2)+6\,{\rm Re}[(B-A)^*C]}. \tag{11}$$

Taking the limit as $s\to 1$ produces a factor of 2, irrespective of A, B, and C. Remembering the neglect of the mass of strange quarks, which can modify decay distributions at $s=1$, we expect the polarization to be approximately twice as large as the forward-backward asymmetry in the region near the upper boundary of the phase space. Another limit for the polarization forward-backward asymmetry is

$$\left.\frac{d\Gamma^{\rm pol}_{\rm FB}/ds}{d\Gamma/ds}\right|_{s\to 0}=-\frac{3}{4}.$$

To extract unambiguously the coefficients relevant to $B\to X_s l^+ l^-$ from measurements is not so straightforward as we might think because they involve observables bilinearly. At this stage, we examine the situation by assuming that A_1, B_1, and C (or F_2) are real, disregarding the likelihood that an imaginary part of them arises from new physics at the weak scale. The assumption does apply to a large number of models. (Strictly speaking, all these coefficients contain the CKM matrix element having a phase factor, but each of them is proportional to $V_{ts}^* V_{tb}$; only does its modulus appear in the observables.) It is interesting that a real $(A-B)$ actually cancels out of numerator and denominator of Eq. (11) for the whole range of s. In this case we may rewrite this ratio as

$$\frac{d\Gamma^{\rm pol}/ds}{d\Gamma_{\rm FB}/ds}=2\,\frac{(1+2s)\,{\rm Re}[(A+B)C]+6C^2}{3s\ {\rm Re}[(A+B)C]+6C^2}. \tag{12}$$

Here we have deliberately put an extra C in both numerator and denominator in order to determine the product ${\rm Re}[(A+B)C]$ experimentally, using C^2 (rather than C) fixed by the $B\to X_s\gamma$ as input, when the data of the polarization along with the forward-backward asymmetry is available. The *linear* dependence on ${\rm Re}[(A+B)C]$ enables us to obtain its size as well as the sign. Note that $(A+B)$ has an imaginary part coming from the one-loop matrix elements of four-quark operators and the resonant contributions, which are given by the measurements of nonleptonic B decays. The imaginary part depends on s and appears in the region above the charm quark threshold $2m_c$.

Next, we move on to the invariant mass distribution from which we may extract the combination $(A-B)$ up to a sign; to obtain the sign, one needs the individual asymmetry. Taking the polarization as an example, we have

$$\frac{d\Gamma^{\rm pol}}{ds}\propto\epsilon_a|(A-B)C|\left((1+2s)\,\frac{{\rm Re}[(A+B)C]}{C^2}+6\right), \tag{13}$$

where ϵ_a stands for the sign of $(A-B)C$ and can be eventually read off once the polarization measurement is carried out. This gives rise to an additional way of measuring the $|A-B|$. (Alternatively, the goal can be achieved by using forward-backward asymmetries.)

Ali, Giudice, and Mannel have proposed a method to obtain coefficients A and B (which are linear combinations of their notations C_9 and C_{10}) using partial integrated decay widths along with forward-backward asymmetries [8]. Their method results in four possible solutions. The advantage of including lepton polarizations, as we have shown above, is that we can work out an *unique* solution to simultaneous equations determined by measured decay width (integrated over a certain kinematic range), polarization, and forward-backward asymmetry. Let us explain it geometrically. The contour line of a given decay width is a ring on the A-B plane. The center of the ring is located on the line $A=B$, but not on the line $A=-B$. The contour line of polarization (forward-backward asymmetry) has two branches; one is associated with a positive $A-B$, while the other with negative $A-B$. When we just combine the width either with polarization or with forward-backward asymmetry, each of these two branches can cross over the ring, resulting in four intersections at most. It is also possible that only one branch crosses over the ring and we end up with two intersections. In such a case, we obtain two values of the combination $A-B$; they are of the same sign, but different magnitudes. Once we put all three sorts of contour lines on the A-B plane, they will intersect at one point. *The failure to intersect indicates that the effective Hamiltonian in Eq. (1) needs to be modified.* As far as signs are concerned, we are able to constrain the relative signs between C and $A-B$ as well as the real part of $A+B$ (or the sign of $A+B$ since the sign of its imaginary part is irrelevant to the observables in question). There is still a free sign which we cannot determine. In fact, under the exchange of $A\to -A$, $B\to -B$, and $C\to -C$ in Eqs. (4)–(7), the decay width along with these asymmetries remain unchanged. It is worthwhile pointing out that the efficiency of our method decreases near the $s\simeq 1$ where, as discussed above, the ratio of leptonic polarizations to forward-backward asymmetries becomes rather insensitive to these coefficients.

A comparison of these experimental outputs with that obtained by model calculations certainly offers a direct test of different models. Nevertheless, we may carry out a model-independent check since we are now in a position to predict the polarization forward-backward asymmetries given in Eq. (7), normalized to the decay width of Eq. (4) without involving specific model calculations. Once again, when we conduct such an analysis we need to be away from $s\simeq 0$ where

this particular asymmetry tends to be independent of the specific values of these coefficients.

V. CONCLUSION

We have investigated lepton distributions in the decay $B\to X_s l^+ l^-$ in number of various models as well as made the analysis in a model-independent way. For model calculations, we summarized the results in Figs. 1–5. For parameters of the extensions of the standard model satisfying constraints placed by direct searchs in collider and by the decay $B\to X_s\gamma$, we still observed large deviations from the standard model predictions in these distributions. We have drawn conclusions which are independent of these models. As well, we have proposed ways to determine the coefficients for the effective Hamiltonian via the measured decay width, polarization, and forward-backward asymmetries. The advantage of our proposal is that both magnitudes and signs of relevant coefficients can be unambiguously extracted from experiments once they become available.

In this work we have assumed lepton distributions in the inclusive process $B\to X_s l^+ l^-$ to be the corresponding ones of the free quark decay $b\to s l^+ l^-$. The scheme is justified by a systematic expansion in inverse powers of the mass of the bottom quark [31,32]. For instance, Falk, Luke, and Savage have evaluated leading corrections to free quark decay and have found that these corrections increase the dilepton invariant mass spectrum by about 10% over the whole range of q^2. Recently, Ali *et al.* reported their calculation of the leading power correction to the dilepton invariant mass spectrum as well as forward-backward asymmetries of the lepton production. They found these distributions to be stable against the corrections, except in the region near the high q^2 end point, where, in contrast with the previous work of Falk *et al.*, they observed a large power correction. Power corrections to leptonic polarization have been calculated lately by Bär and Pott who take a different value of the parameter λ_1 from that used in the work of Falk *et al.*; they have shown the correction to the free quark decay is at most 3.5% for $q^2>0.4m_b^2$ and 5.2% for $q^2\simeq 0.1m_b^2$ [33]. They also found a small power correction for the invariant mass spectrum, compared with what Falk *et al.* suggested. With respect to lepton polarization forward-backward asymmetry we do not expect the correction to be substantial in the small and medium q^2 region.

ACKNOWLEDGMENTS

The authors are grateful to the Australian Research Council for their financial support, under Grant No. A69231484. We also thank N. R. Jones for his assistance in using MATHEMATICA.

APPENDIX: SHORT-DISTANCE COEFFICIENTS IN EXTENSIONS OF THE STANDARD MODEL

We present short-distance coefficients A_1', B_1', and F_2' arising from extensions of the standard model. For the amplitude of loop diagrams with charged Higgs bosons, we have

$$A_1'=B_1'-v_{21}^2 x b(y),$$

$$B_1'=v_{21}^2[2x b(y)+f(y)]s_W^2, \tag{A1}$$

with $y=m_t^2/M_{H^-}^2$, where $b(y)$ represents the contribution of Z penguin diagrams and $f(y)$ comes from photon ones. Also, photon penguin diagram give rise to

$$F_2'=2v_{21}^2\eta^{-16/23}\Big(g(y)-\tfrac{1}{6}\ a(y)+\tfrac{8}{3}\ (\eta^{2/23}-1) \times[h(y)-\tfrac{1}{6}\ e(y)]\Big), \tag{A2}$$

in models of type I. The box diagrams with t-H^--ν loops are negligible due to the weak Yukawa coupling of leptons. In model II, A_1' and B_1' remain unchanged, but

$$F_2'=-2\eta^{-16/23}\left(g(y)+\frac{v_{21}^2}{6}\ a(y)+\frac{8}{3}(\eta^{2/23}-1) \times\left[h(y)+\frac{v_{21}^2}{6}\ e(y)\right]\right). \tag{A3}$$

An interesting property of F_2' is that in the latter case, it does not vanish with v_{21}. The various functions appearing in the above equations are listed below:

$$a(y)=-\frac{y}{2}\left[\frac{1}{6}\frac{8y^2+5y-7}{(1-y)^3}+\frac{3y^2-2y}{(1-y)^4}\ \ln y\right], \tag{A4}$$

$$b(y)=\frac{y}{4}\left[\frac{1}{1-y}+\frac{1}{(1-y)^2}\ \ln y\right], \tag{A5}$$

$$e(y)=-\frac{y}{2}\left[\frac{1}{2}\frac{y^2-5y-2}{(1-y)^3}-\frac{3y}{(1-y)^4}\ \ln y\right], \tag{A6}$$

$$f(y)=\frac{y}{18}\left[\frac{1}{6}\frac{47y^2-79y+38}{(1-y)^3}+\frac{3y^3-6y+4}{(1-y)^4}\ \ln y\right], \tag{A7}$$

$$g(y)=\frac{y}{6}\left[\frac{1}{2}\frac{5y-3}{(1-y)^2}+\frac{3y-2}{(1-y)^3}\ \ln y\right], \tag{A8}$$

$$h(y)=\frac{y}{2}\left[\frac{1}{2}\frac{y-3}{(1-y)^2}-\frac{1}{(1-y)^3}\ \ln y\right]. \tag{A9}$$

Now we move on to loop diagrams containing charginos. We use the notations $\widetilde{F}_1$ and $\widetilde{F}_2$ to represent the monopole and dipole form factors, respectively, for the photon penguin diagram with chargino-up-squark loops. As well, $\widetilde{C}^{\rm Z}$ and $\widetilde{C}^{\rm box}$ denote the contributions of Z penguin and box diagrams (both of which contain chargino-up-squark loops). Then, in addition to the effect of charged Higgs bosons in model II, we have

$$A_1'=B_1'+\widetilde{C}^{\rm Z}+\widetilde{C}^{\rm box}, \tag{A10}$$

$$B_1'=-s_W^2(\widetilde{F}_1+2\widetilde{C}^{\rm Z}), \tag{A11}$$

and the dipole form factor F_2' is augmented by

$$\widetilde{F}_2 = -4\eta^{-16/23}\sum_{j=1}^{2}\frac{M_W^2}{M_{\chi_j}^2} \times\sum_{k=1}^{6}\mathcal{M}_{jk}\left[\mathcal{R}_{jk}g(z_{kj})-\frac{\mathcal{N}_{jk}}{6}\,a(z_{kj})\right], \quad \text{(A12)}$$

with $z_{kj}=m_{\widetilde{U}_k}^2/M_{\chi_j}^2$, where $m_{\widetilde{U}_k}$ and M_{χ_j} stand for the mass of the six up squarks and two charginos, respectively. $\mathcal{M}$, $\mathcal{N}$, and $\mathcal{R}$ are made up of various mixing matrices which transform weak interaction eigenstates into mass ones. Under the circumstance where we just account for the dominant mixing between the left- and right-handed supersymmetry partners of top quarks, $\widetilde{t}_L$ and $\widetilde{t}_R$, the mass eigenstate of up squarks reads

$$\widetilde{U}_k=(\widetilde{u}_L,\widetilde{c}_L,\widetilde{t}_1,\widetilde{u}_R,\widetilde{c}_R,\widetilde{t}_2). \quad \text{(A13)}$$

Thus one has

$$\mathcal{M}_{jk}=\left[-V_{j1}K_{us}^*,\ -V_{j1}K_{cs}^*,\ \left(-V_{j1}c_{\tilde{t}}+\frac{m_t}{\sqrt{2}M_W\sin\beta}\,V_{j2}s_{\tilde{t}}\right)K_{ts}^*,\ \frac{m_u}{\sqrt{2}M_W\sin\beta}\,V_{j2}K_{us}^*,\ \frac{m_c}{\sqrt{2}M_W\sin\beta}\,V_{j2}K_{cs}^*,\ \left(V_{j1}s_{\tilde{t}}+\frac{m_t}{\sqrt{2}M_W\sin\beta}\,V_{j2}c_{\tilde{t}}\right)K_{ts}^*,\right], \quad \text{(A14)}$$

and $\mathcal{N}_{jk}$ (associated with the incoming bottom quark line) is obtained by replacement of K_{qs}^* by the corresponding K_{qb} (we use K to stand for the CKM matrix in this Appendix). Moreover, we have

$$\mathcal{R}_{jk}=\frac{m_b}{\sqrt{2}M_W\cos\beta}\,U_{j2}[K_{ub},K_{cb},c_{\tilde{t}}K_{tb},0,0,-s_{\tilde{t}}K_{tb}]. \quad \text{(A15)}$$

Here $s_{\tilde{t}}(c_{\tilde{t}})$ stands for $\sin\widetilde{\theta}_t(\cos\widetilde{\theta}_t)$, $\widetilde{\theta}_t$ being the mixing angle between $\widetilde{t}_L$ and $\widetilde{t}_R$. V along with U transform the W-ino and Higgsino (the supersymmetric partners of the W boson and the charged Higgs boson), which are interaction eigenstates, into the charginos that are mass eigenstates. We may safely overlook the weak mixing between supersymmetric magnetic and chromomagnetic operators if the latter is not particularly large.

It is worthwhile noting the property of a Glashow-Iliopoulos-Maiani (GIM)-like cancellation (with unitarity of the CKM matrix) possessed by $\widetilde{F}_2$. As demonstrated explicitly by Garisto and Ng [30], the $\mathcal{R}$-related part of $\widetilde{F}_2$ disappears when all up-type squarks involved have the same mass. But we point out that the $\mathcal{N}$-related part (and $\widetilde{F}_1$ given below) vanishes only if the up-type quarks are degenerate.

The photon penguin diagram (with the chargino-up-squark loop), in addition to dipole form factor, gives rise to the monopole form factor

$$\widetilde{F}_1=\frac{2}{3}\sum_{j=1}^{2}\frac{M_W^2}{M_{\chi_j}^2}\sum_{k=1}^{6}\mathcal{M}_{jk}\mathcal{N}_{jk}\widetilde{d}(z_{kj}), \quad \text{(A16)}$$

where $\widetilde{d}$ is defined as

$$\widetilde{d}(z)=-\frac{1}{6}\left[\frac{1}{6}\,\frac{52z^2-101z+43}{(1-z)^3}+\frac{6z^3-9z^2+2}{(1-z)^4}\,\ln z\right]. \quad \text{(A17)}$$

It is associated with a vector lepton current and thus contributes to A_1' and B_1' equally. We can read off a logarithmic dependence of $\widetilde{d}(z)$ on small z. This indicates a potentially large effect of the lightest up-type squark such as the top squark. However, such a logarithmic enhancement may manifest itself only for a lightest top squark with a mass less than the W mass.

The coefficient arising from the box diagrams, $\widetilde{C}^{\rm box}$, is given by

$$2\sum_{i,j=1}^{2}\frac{M_W^2}{M_{\chi_j}^2}\sum_{k=1}^{6}\mathcal{M}_{jk}\mathcal{N}_{ik}V_{i1}V_{j1}\xi(z_{kj},z_{ki}/z_{kj},z_{lj}), \quad \text{(A18)}$$

with $z_{lj}=m_{\tilde{\nu}}^2/M_{\chi_j}^2$ and

$$\xi(z_1,z_2,z_3)=\frac{z_1^2\ln z_1}{(z_1-1)(z_1-z_2)(z_1-z_3)}+z_1\leftrightarrow z_2+z_1\leftrightarrow z_3. \quad \text{(A19)}$$

It contributes only to the left-handed current of leptons and ought to be added to A_1'. Like the ordinary neutrino, the sneutrinos $\widetilde{\nu}$ appear in the box diagrams, and when we restrict ourselves to e and μ channels only the first two generations of sneutrinos, which are assumed to be degenerate with a mass $m_{\tilde{\nu}}$, are involved. The function ξ is not bounded when all z_i are simultaneously small. To reveal the feature we examine a special case of $z_1=z_2=z_3=z$, where ξ reduces to

$$\xi(z)=\frac{z-3}{2(z-1)^2}+\frac{\ln z}{(z-1)^3}. \quad \text{(A20)}$$

Obviously, it goes logarithmically with a vanishing z. Nevertheless, once again the factor of $M_W^2/M_{\chi_j}^2$ can reduce the contribution with small z_i. When up-type squarks are degenerate $\widetilde{C}^{\rm box}$ also experiences a GIM-like cancellation, provided that the two charginos have the same mass or do not mix or if the quarks of up type are mass degenerate.

Finally, the short-distance coefficient arising from Z penguin diagrams takes the form

$$\widetilde{C}^Z=\frac{1}{4}\sum_{i,j=1}^{2}\sum_{k,k'=1}^{6}\mathcal{M}_{ik}\mathcal{N}_{jk'}[-\delta_{ij}\gamma_{kk'}\xi_1(z_{kj},z_{k'j}) + \delta_{kk'}V_{i1}V_{j1}\xi_2(z_{ki},z_{kj})+\delta_{kk'}U_{i1}U_{j1}\xi_3(z_{ki},z_{kj}), \tag{A21}$$

where $\gamma_{kk'}=\gamma_k\delta_{kk'}-c_{\tilde{t}}s_{\tilde{t}}(\delta_{k3}\delta_{k'6}+k\leftrightarrow k')$ and $\gamma_k=(1,1,c^2_{\tilde{t}},0,0,s^2_{\tilde{t}})$. Also, we define above three (positive definite) functions as

$$\xi_1(z_1,z_2)=\frac{z_1^2\,\ln z_1}{(z_1-1)(z_1-z_2)}+z_1\leftrightarrow z_2, \tag{A22}$$

$$\xi_2(z_1,z_2)=\frac{\ln z_1}{2(z_1-1)(z_2-1)}\left(z_1z_2-\frac{z_1^2+z_2^2-z_1-z_2}{z_1-z_2}\right) + z_1\leftrightarrow z_2, \tag{A23}$$

$$\xi_3(z_1,z_2)=-2\sqrt{z_1z_2}\,\frac{\ln z_1}{(z_1-1)(z_1-z_2)}+z_1\leftrightarrow z_2. \tag{A24}$$

Note that ξ_1 and ξ_2 increase logarithmically with large z_1 or z_2, while ξ_3 decreases. To illustrate the situation we consider a special case of $z_1=z_2=z$, where ξ_i's reduce to

$$\xi_1(z)=z\left(\frac{1}{z-1}+\frac{z-2}{(z-1)^2}\,\ln z\right), \tag{A25}$$

$$\xi_2(z)=-\frac{1}{z-1}+\frac{z^2}{(z-1)^2}\,\ln z, \tag{A26}$$

$$\xi_3(z)=-\frac{2}{z-1}+\frac{2z}{(z-1)^2}\,\ln z. \tag{A27}$$

Clearly, as z becomes large, $\xi_{1,2}$ become $\ln z$, while ξ_3 is vanishing. We have checked the GIM-like cancellation for $\widetilde{C}^Z$. If all up-type squarks have the same mass, the $\gamma_{kk'}$ term disappears directly as does the $V\otimes V$ term with the same additional conditions which apply to $\widetilde{C}^{\rm box}$. However, for degenerate squarks and charginos as well, the $U\otimes U$ term cancels out only when the W-ino–Higgsino mass matrix is symmetric, namely, $\tan\beta=1$. This will be badly broken by a large $\tan\beta$.

Note that $\mathcal{M}_{jk}$ (and $\mathcal{N}_{jk}$) for $k=4,5$ are effectively suppressed, which violates the GIM-like cancellation for $\widetilde{F}_1$ and partially for $\widetilde{F}_2$. In this work we neglect them and thus the contributions of the right-handed supersymmetric partners of up and charm quarks. Applying unitarity of the CKM matrix we may further isolate a particular part of these coefficients such that it is determined by the mass difference of the left-handed supersymmetric partners of up and charm quarks, but suppressed by $K_{ub}K^*_{us}$. Thus we can safely ignore this part as long as $|m_{\tilde{c}_L}-m_{\tilde{u}_L}|<|m_{\tilde{t}_{1,2}}-m_{\tilde{c}_L}|$ is satisfied. As a result, we end up with coefficients proportional to $K_{tb}K^*_{ts}$; they depend explicitly upon six masses $m_{\tilde{c}_L}$, $m_{t_{1,2}}$, $m_{\chi_{1,2}}$, and $m_{\tilde{\nu}}$, as well as three mixing angles $\widetilde{\theta}_t$, $\widetilde{\theta}_V$, and $\widetilde{\theta}_U$; the latter two angles apply to the W-ino and Higgsino.

[1] CLEO Collaboration, R. Ammar *et al.*, Phys. Rev. Lett. **71**, 674 (1993); B. Barish *et al.*, *ibid.* **74**, 2885 (1995).

[2] J. L. Hewett, in *Spin-Structure in High Energy Processes*, Proceedings of the 21st SLAC Summer Institute, Stanford, California, 1993, edited by L. De Porcel and C. Dunwoodie (SLAC Report No. 444, Stanford, 1994).

[3] CLEO Collaboration, B. Balest *et al.*, Report No. CLEO CONF 94-4 (unpublished); CDF Collaboration, C. Anway-Wiese, in *The Albuquerque Meeting*, Proceedings of the Meeting of the Division of Particles and Fields of the APS, Albuquerque, New Mexico, 1994, edited by S. Seidel (World Scientific, Singapore, 1993).

[4] Dongsheng Liu and R. Delbourgo, Phys. Rev. D **53**, 548 (1996).

[5] J. L. Hewett, Phys. Rev. D **53**, 4964 (1996).

[6] A. Ali, T. Mannel, and T. Morozumi, Phys. Lett. B **273**, 505 (1991).

[7] R. Delbourgo and Dongsheng Liu, Phys. Rev. D **51**, 118 (1995).

[8] A. Ali, G. F. Giudice, and T. Mannel, Z. Phys. C **67**, 417 (1995).

[9] Dongsheng Liu, Phys. Lett. B **346**, 355 (1995); Phys. Rev. D **52**, 5056 (1995).

[10] P. Cho, M. Misiak, and D. Wyler, Phys. Rev. D **54**, 3329 (1996).

[11] C. Greub, A. Ioannissian, and D. Wyler, Phys. Lett. B **346**, 149 (1995).

[12] B. Grinstein, M. J. Savage, and M. B. Wise, Nucl. Phys. **B319**, 271 (1989); R. Griganis, P. J. O'Donnell, M. Sutherland, and H. Navelet, Phys. Lett. B **223**, 239 (1989); G. Cella, G. Ricciardi, and A. Vicere, *ibid.* **258**, 212 (1991).

[13] N. G. Deshpande, K. Panose, and J. Trampetic, Phys. Lett. B **308**, 322 (1993).

[14] N. G. Deshpande and J. Trampetic, Phys. Rev. Lett. **60**, 2583 (1988).

[15] T. Inami and C. S. Lim, Prog. Theor. Phys. **65**, 297 (1981).

[16] M. Misiak, Nucl. Phys. **B393**, 23 (1993); **B439**, 461(E) (1995).

[17] A. J. Buras and M. Muenz, Phys. Rev. D **52**, 186 (1995).

[18] N. G. Deshpande, J. Trampetic, and K. Panose, Phys. Rev. D **39**, 1461 (1989); C. S. Lim, T. Morozumi, and A. I. Sanda, Phys. Lett. B **218**, 343 (1989); C. A. Dominguez, N. Paver, and Riazuddin, Z. Phys. C **48**, 55 (1990).

[19] Particle Data Group, R. M. Barnett, *et al.* Phys. Rev. D **54**, 1 (1996).

[20] R. G. Ellis, G. C. Joshi, and M. Matsuda, Phys. Lett. B **179**, 119 (1986).

[21] B. Grinstein and M. B. Wise, Phys. Lett. B **201**, 274 (1988).

[22] Wei-Shu Hou and R. S. Willey, Phys. Lett. B **202**, 391 (1988).

[23] B. Grinstein, M. J. Savage, and M. B. Wise, Nucl. Phys. **B339**, 26 (1990).

[24] C-H. Chang and C. Lü, Report No. AS-ITP-95-23, hep-ph/9507384 (unpublished).

[25] J. L. Hewett, Phys. Rev. Lett. **70**, 1045 (1993); V. Barger, M.

S. Berger, and R. Phillips, *ibid.* **70**, 1368 (1993).
[26] S. Bertolini, F. Borzumati, and A. Masisero, Nucl. Phys. **B353**, 591 (1991).
[27] See, for example, A. B. Lahanas and D. V. Nanopoulos, Phys. Rep. **145**, 1 (1998); H. E. Haber and G. L. Kane, *ibid.* **117**, 75 (1987).
[28] Numerically, we adopted $\alpha_X = 1/24.11$ and $M_X = 10^{16.187}$ GeV obtained in J. Wu, R. Arnowitt, and P. Nath, Phys. Rev. D **51**, 1371 (1995).
[29] R. Barbieri and G. F. Giudice, Phys. Lett. B **309**, 86 (1993).
[30] R. Garisto and J. N. Ng, Phys. Lett. B **315**, 372 (1993).
[31] A. F. Falk, M. Luke, and M. J. Savage, Phys. Rev. D **49**, 3367 (1994).
[32] A. Ali, G. Hiller, L. T. Handoko and T. Morozumi, Phys. Rev. D **55**, 4105 (1997).
[33] O. Bär and N. Pott, Phys. Rev. D **55**, 1684 (1997).